Javier MARTINEZ[1], Anouar BELAHCEN[1,2], Antero ARKKIO[1]

Aalto University, Dept. of Electrical Engineering (1), Tallinn University of Technology, Dept. of Fundamentals of Electrical Engineering and Electrical Machines (2)

A 2D FEM model for transient and fault analysis of induction machines

Abstract. *This paper presents the basic guidelines to develop a coupled FEM for the study of electromagnetic phenomena in induction motors. FEM model is formulated using the 2D magnetic vector potential. FEM model presented inside of this work presents a formulation where external circuits can be also coupled. Furthermore, the model takes into account the end effects of the end-winds and end-rings of the electrical device.*

Streszczenie. *W artykule przedstawiono podstawowe wytyczne do opracowania za pomocą FEM sprzężonego modelu do badania zjawisk elektromagnetycznych w silnikach indukcyjnych. Model został opracowany przy użyciu wektorów potencjałów magnetycznych w 2D. Przedstawiony model formułuje możliwości dołączenia obwodów zewnętrznych. Model uwzględnia również efekty brzegowe na skrajach uzwojeń i pierścieni (**Model 2D FEM do analizy stanów przejściowych i stanów awaryjnych maszyn indukcyjnych)***

Keywords: FEM, induction motor, transient state
Słowa kluczowe: FEM, silnik indukcyjny, stan przejściowy

Introduction

Many industrial processes and applications require the ability to ensure induction motors are operating in a satisfactory way. For this reason, it is important to develop accurate models to help the understanding of the occurring electromagnetic phenomena. As it is stated in [1], sources of machine faults can be considered to be either of internal or external nature. Common internal sources of fault are due to the crack of rotor bars [2] or dielectric failure in the stator winding coils [3]. On the other hand, external sources are normally due to problems concerning to anomalies in the supply [4].

FEM models are excellent computational tools which allow us to overcome the solution for difficult geometric entities such as slots and non-linearities such as iron constitutive law.

In addition to the previous advantages, current commercial codes allow to extend the analysis of electromagnetic field equations together with other physical phenomena occurring in the induction motor [5]. This advantage allows us the possibility to develop the different techniques for the analysis of faults.

Most popular analysis techniques are based on stator current analysis. This method is characterized to be non-intrusive, but one of the drawbacks is to sense current using hall sensors without disturbances. [6] shows that analysis techniques can also be based on vibration monitoring, temperature measurement, motor torque and speed harmonic analysis.

This paper is divided into four sections. In section II, we develop the basic equations for a 2D electromagnetic model. In section III, we present basic results of this model. Last section deals with conclusions.

Basic FEM formulation

This section provides the basic formulation for a transient electromagnetic model. Full geometry of the induction motor must be considered in case faults are supplied into the system. Within the model, Kirchoff's laws have been coupled in order to be able to supply the induction machine using voltage sources. In addition to the capability of coupling external circuits to the model, kinematic and rotor movement is also considered. The movement of the rotor differs from the formulation appearing in [7]-[8]. The movement follows the formulation stated in [9]. This section is divided into three parts. First subsection analyses stator domain and its coupling with the grid. Second subsection, describes the field equations in rotor domain and describes the end effects of a squirrel cage rotor. Last subsection deals with the coupling of motion.

Stator Domains

Stator of induction motors is formed by laminated iron sheets, slots of filamentary winding and half of the air-gap. This can be expressed as in eq. (1).

$$\Omega_{stator} = \Omega_{iron} \cup \Omega_{slot} \cup \Omega_{\frac{ag}{2}} \tag{1}$$

Ω_{iron} being the domain comprised of iron sheet, Ω_{slot} slot being the domain comprised of stator slots and $\Omega_{\frac{ag}{2}}$ being half of the air-gap. Fig. 1 illustrates these domains in the cross-section of an induction motor.

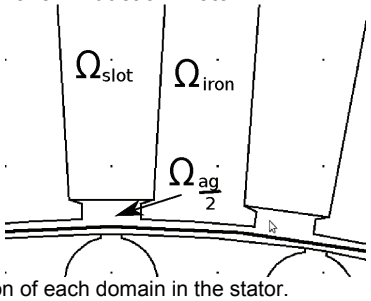

Fig.1. Definition of each domain in the stator.

Field equations are formulated as (2)-(4)

$$\nabla \times \left(\frac{1}{\mu_{iron}} \nabla \times a_z \right) = 0 \quad on \quad \Omega_{iron} \tag{2}$$

$$\nabla \times \left(\frac{1}{\mu_0} \nabla \times a_z \right) = \frac{N i_\phi \hat{e}_z}{A_{slot}} \quad on \quad \Omega_{slot} \tag{3}$$

$$\nabla \times \left(\frac{1}{\mu_0} \nabla \times a_z \right) = 0 \quad on \quad \Omega_{\frac{ag}{2}} \tag{4}$$

a_z being the z-component of magnetic vector potential. i_ϕ is the phase current and N being the number of turns.

Equation (3) shows that i_ϕ is an unknown when the induction motor is supplied by a voltage source. In this case, an extra equation can be formulated using the connection between the supply and terminals of the induction motor. This can be expressed for star connection using Kirchoff Current Law.

$$(5)\quad v_\phi - v_{emf} = R_{end\ wind} i_\phi + L_{end\ wind} \frac{di_\phi}{dt}$$

v_ϕ being voltage supply, v_{emf} back electromotive force in each coil and $L_{end\ wind}$, $R_{end\ wind}$ takes into account the end effects of the 2D magnetodynamic model. The per phase circuit corresponding to (5) is shown in Fig. 2.

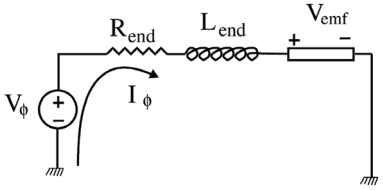

Fig. 2. Coupling between external voltage supplies and FEM 2D model. This loop represents one phase of the stator.

Back-emf for filamentary windings can be expressed using [8] as:

$$(6)\quad v_{emf} = \frac{-Nl_{motor}}{A_{slot}} \int_{\Omega_{slot}} \frac{da_z}{dt} d\Omega_{slot}$$

The outer interface between stator yoke and air must be considered as a magnetic insulation. Thus, it gives the following boundary condition.

$$(7)\quad a_z = 0 \quad on \quad \partial\Omega_{iron}$$

Rotor Domains

Rotor of induction machines can be decomposed in the following domains into the FEM model.

$$(8)\quad \Omega_{rotor} = \Omega_{iron} \cup \Omega_{al} \cup \Omega_{\frac{ag}{2}} \cup \Omega_{shaft}$$

Ω_{al} al being the domain of rotor bars and Ω_{shaft} shaft being the domain taking into account the iron shaft characteristics.

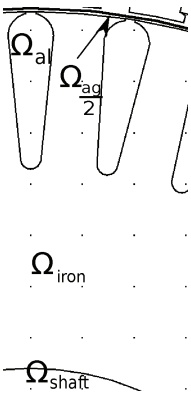

Fig. 3. Definition of each domain in the rotor.

Field equations for each domain are defined in (9)-(10) as

$$(9)\quad \nabla \times \left(\frac{1}{\mu_{iron}} \nabla \times a_z \right) + \sigma \frac{da_z}{dt} = \sigma \frac{\Delta v_i}{l_{motor}} \quad on \quad \Omega_{al}$$

$$(10)\quad \nabla \times \left(\frac{1}{\mu_{shaft}} \nabla \times a_z \right) + \sigma \frac{da_z}{dt} = 0 \quad on \quad \Omega_{shaft}$$

The term appearing in (9)-(10) takes into account the eddy currents induced in solid conductors. Last term in (9) takes into account the end effect of the rotor cage. Δv_i represents the voltage difference between consecutive bars in the rotor. Thus, the term Δv_i, appearing in eq. (9), is also another unknown variable that can be solved according to the circuit topology of the squirrel cage. Kirchoff Voltage Law for consecutive bars is

$$(11)\quad v_i - v_{i+1} = 2\left(R_{ring\,i} i_{loop\,i} + L_{ring} \frac{di_{loop\,i}}{dt} \right)$$

v_i and v_{i+1} represents the i-th and i+1-th bar voltage respectively. R_{ring} and L_{ring} are the end ring impedances of the rotor cage. The current among loops can also be expressed as a function of the current in the rotor bars as as in eq. (12). Such an approach is illustrated in the circuit of Fig. 4.

$$(12)\quad i_{alu,i} = i_{loop,i} - i_{loop,a+1}$$

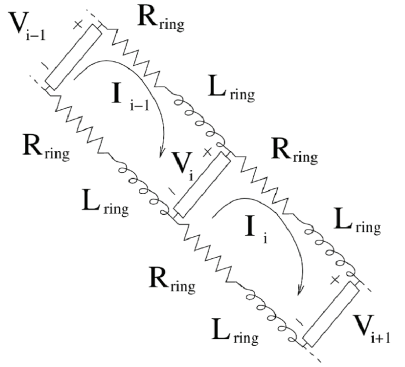

Fig. 4. Loop topology of the rotor bars. Each loop represents the connection between consecutive bars. Loops are connected through the end ring impedances.

Finally, every bar current flowing inside of the bar can be expressed as

$$(13)\quad i_{alu,i} = \frac{v_{alu,i}}{R_{alu,i}} - \int_{\Omega_{alu,i}} \sigma \frac{da_z}{dt} d\Omega_{alu,i}$$

Coupling Kinematic Equations and Movement

Movement of the rotor is a consequence of the creation of a stress tensor in the air-gap. Due to this stress along the boundary of the rotor-airgap, a torque is produced. It can be expressed as

$$(14)\quad F_{rotor} = \oint_{\Omega_{rotor}} \sigma_{MST} \cdot \hat{n} d\Omega_{rotor}$$

σ_{MST} being the Mawell Stress Tensor defined in [7]. The definition of the surface integral can be simplified for 2D electromagnetic models taking into the account the fact that the flux is axially constant.

(15) $$d\Omega_{rotor} = d\Gamma_{rotor} \times d\hat{z} = l_{rotor}\hat{e}_z \times d\Gamma_{rotor}$$

$d\Omega_{rotor}$ rotor being the differential surface, $d\Gamma_{rotor}$ rotor being the differential boundary length and $d\hat{z}$ the differential length in axial direction. This approach is illustrated in Fig. 5. Substituting (15) into (14), we obtain the total force and torque for a sliced model as

(16) $$F_{rotor} = \oint_{\Gamma_{rotor}} \sigma_{MST} \cdot \hat{n} l_{rotor} d\Gamma_{rotor}$$

(17) $$T_{rotor} = \left(\oint_{\Gamma_{rotor}} \hat{r} \times (\sigma_{MST} \cdot \hat{n}) l_{rotor} d\Gamma_{rotor} \right)$$

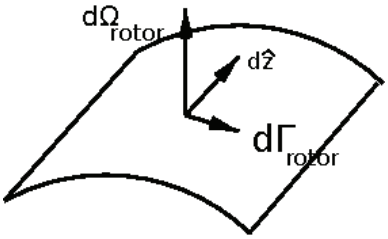

Fig. 5. Geometric description of the rotor surface. The surface vector is defined as the curl of two directors vectors.

The movement in the motor is determined by the kinematic relationship

(18) $$T_{rotor} - T_{load} = J_{rotor} \frac{d^2\theta}{dt^2}$$

J_{rotor} being the moment of inertia and θ being its angular position. As a last step, the solution of stator and rotor domains must be continuous and follow the movement of the rotor. This constraint can be achieved by using a Lagrange multiplier in the common boundary between both domains [9].

Results

In order to prove the previous formulation, we implemented and used a FEM commercial software (Comsol). The induction motor has 48 stator slots and 40 cast aluminium bars. Stator and rotor are made of laminated iron. Details are summarized in Table I .The shaft is considered to be of solid iron with losses. Details of the mesh and numerical solvers are given in Table 2. Since the purpose of this model is to be able of simulating faults, symmetry conditions have been neglected.

Start-up of the induction motor has been simulated. Therefore, all initial conditions in the motor are equal to zero. In Fig. 6, we can see the induction machine during the first moments of the starting. Flux is not penetrating inside of the rotor since bars are carrying high currents. As a result, edges of the slots, which are included inside of the iron do- mains, are highly saturated. Nevertheless, the rest of iron behaves as a linear material. Thus, the relative permeability of the iron is high. This effect can be clearly seen in Fig. 6. Flux lines are not capable of penetrating because of the ratio of relative permeabilities between iron and airgap. Oppositely, Fig. 7 shows flux and equipotential lines after reaching steady state. Flux can penetrate inside of the rotor since the difference between the rotating field and rotational speed is so small that rotor bars are not capable of inducing any current. It can be seen this phenomena by appreciating that flux lines are not distorted when they enter into the rotor parts. It can also be stated that iron inside of the rotor is partly saturated $(1 \le |B| \le 1{,}5\,T)$.

In Fig. 8, we can see the rotational speed is having a characteristic of a second-order system having an overshoot. The air-gap torque is having a high number of harmonics. These harmonics are due to the distribution of stator current in slots. This characteristic can also be appreciated in the stator phase currents. There are several reasons for the existence of such harmonics. The distribution of the several phases in several coils creates harmonics in the rotating field appearing on the airgap rotating flux. These high-order harmonics can be filtered if the rotor bars are skewed a certain angle. Thus, one of the main limitations of a 2D model is the impossibility of modelling the aforementioned skew. Another source of harmonics in the torque comes in the slot opening of the stator. This effect is explained in [10]. Fig. 10 shows stator phase currents. We can observe that during the moment where the rotational speed of the rotor is small stator currents are large. The reason for this is to maintain the flux in the air gap. During early moments, rotor bars try to oppose to the flux created by the stator as a consequence of Faraday's law. As the speed increases, the flux variation inside of the rotor decreases and the emf created in the bars decreases in the same manner.

Table 1. Data of the Induction Motor Used within Fem

Motor Type	Induction
Connection	Star
Nominal Voltage	380V
Supply Frequency	100[Hz]
Stator Slots	48
Rotor Slots	40

Table 2. FEM characteristics and parameters

Type of Element	Triangular
Order	Quadratic Elements
Number of Elements	24296
Number of Unknowns	51979
Time Integration Scheme	Linear MultiStep Method
Max. Integration Order	4
Time Step	0.1ms
Non-linear Solver	Damping Newton Method

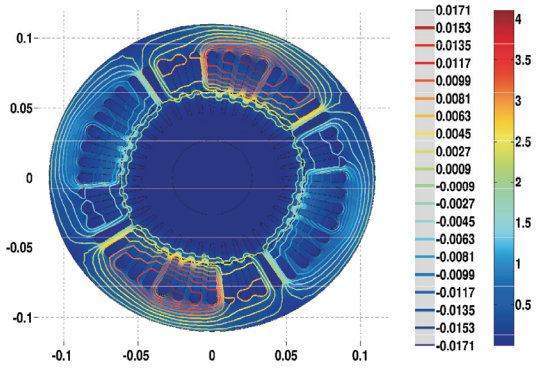

Fig. 6. Flux density and equipotential lines during the first moments at start-up. Time = 1 ms. The left scale is for the vector potential and the one on the right is for the magnetic flux density.

Discussion

As the results show, a 2D electromagnetic model of the induction motor settles a good framework for the study of faults. The inclusion of circuit equations to the system allows the possibility to model both internal and external fault electrical sources. From a modeling point of view, a 2D

electromagnetic model including the end effects of both end windings and end rings represents with accuracy all the non-linearities along the slots. The main drawback of this model comes when the rotor is skewed in order to filter all harmonics produced by the airgap. Furthermore, further analysis of faults can be easily extended adding few modifications.

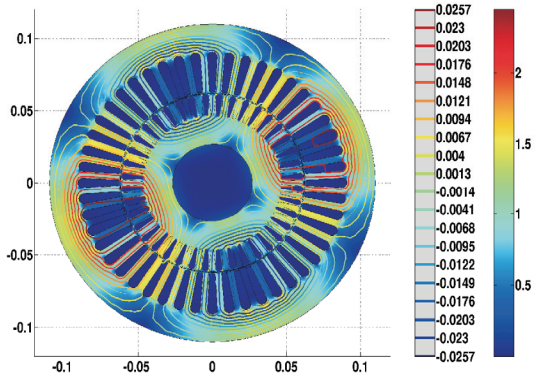

Fig. 7. Flux density and equipotential lines after reaching steady-state. Time = 0,1s. The left scale is for the vector potential and the one on the right is for the magnetic flux density.

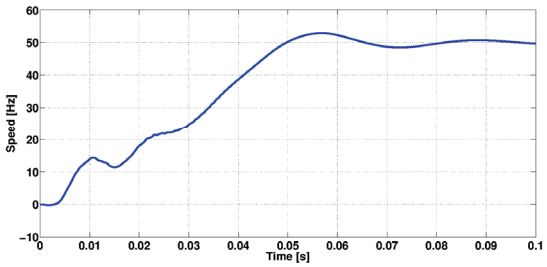

Fig. 8. Rotational speed.

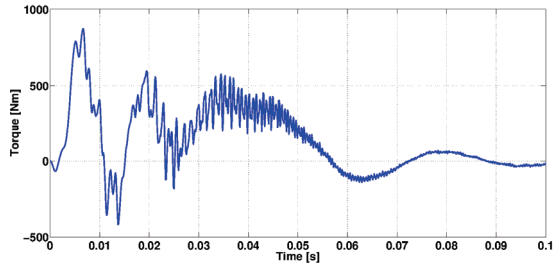

Fig. 9. Rotor torque calculated using Maxwell Stress Tensor.

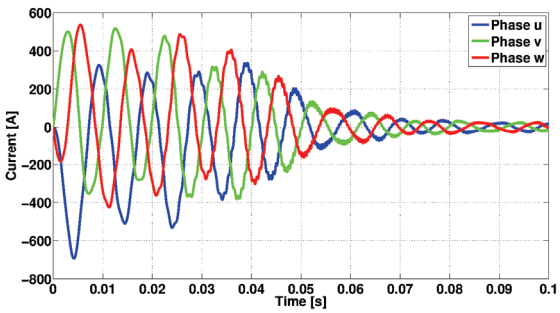

Fig. 10. Stator phase currents at start of the machine from stand still.

In order to model static eccentricity, by shifting the rotor and remeshing we can employ the same formulation. For the case of dynamic eccentricity, we should change the previous remeshing we can employ the same formulation. shifting by a time-dependent parameter. Electric faults inside of the motors can be done in an easy way. A phase short circuit can be easily done by connecting two stator phases in 2 under the same voltage supply. Broken rotor bars can be implemented by estimating zero conductivity in one of the rotor bars. Stator faults can be implemented by joining the back-emf of couple of slots, appearing in eq. (6), by a short-circuit resistance.

In case we are willing to implement a vibration analysis, we could use σ_{MST} as input stress for the elastodynamic equation. On the other hand, we could also use electric power and losses, coming from the electromagnetic model, as input to the heat transfer equations. In this way, we could be able to detect hot spots produced by faults.

Acknowledgement

The authors thank Prof. Tapani Jokinen for the encouraging comments. The authors would also like to express their gratitude to the FOVI project for the funding.

The publication of this paper was supported by the European Social Fund (project "Doctoral School of Energy and Geotechnology II").

REFERENCES

[1] G.K. Singh, S. Al Kazzaz: Induction Machine Drive Condition Monitoring and Diagnostic Research, Electric Power Systems Research, vol. 64, pp. 145–158, Aug 2002.

[2] F.Filipetti, G.Franceschini et al.: AI Techniques in Induction Machines Diagnosis Including the Speed Ripple Effect, IEEE Trans. on Industry Applications, vol. 34, pp. 98–108, Jan/Feb 1998.

[3] R.M. Tallam et al.: Transient Model for Induction Machines with Stator Winding Turn Faults, IEEE Trans. on industry applications, vol.38, May/June 2002.

[4] J.O. Estima, A.J. Cardoso, Performance Analysis of Permanent Magnet Synchronous Motor Drives under Inverter Fault Conditions, Proc. ICEM. 2008.

[5] R.J Belmans et al., Electro-mechanical Analysis of the Audible Noise of an Inverter Fed-Squirrel-cage Induction Motor, IEEE Trans. on Inductrial Applications, vol.27, no.2, pp. 539–544, May/June 1991.

[6] A. Lebaroud, G. Clerg, Diagnosis of Induction Motor Faults using Instantaneous Frequency Signature, 2008.

[7] A. Arkkio, Analysis of Induction Motors Based on the Numerical Solution of the Magnetic field and circuit equations, PhD Thesis, Helsinki University of Technology, 1987.

[8] J.P. Bastos, N. Sadowski, Electromagnetic Modeling by Finite Element Methods 1st ed, CRC Press 2003.

[9] D. Rodger, H.C.Lai, P.J.Leonard., Coupled Elements for Problems Involving Movement, IEEE trans. on magnetics, vol.26, pp. 548-550, March 1990.

[10] B. Heller, V. Hamata Harmonic Field Effects in Induction Machines, 1977, Elsevier.

***Authors**: M. Sc. Javier Martinez, Prof. A. Belahcen, Prof. A. Arkkio, School of Electrical Engineering, Department of Electrical Engineering, Faculty of Electrical Engineering, Aalto University, Otakaari 5A, FI-02150, Espoo, Finland. Email: javier.martinez@aalto.fi,anouar.belahcen@aalto.fi, antero.arkkio@aalto.fi*